Geosci. Model Dev. Discuss., https://doi.org/10.5194/gmd-2017-164
Manuscript under review for journal Geosci. Model Dev.
Discussion started: 14 August 2017

Geoscientific Model Development Discussions

Prognostic parameterization of cloud ice with a single category in the aerosol-climate model ECHAM(v6.3.0)-HAM(v2.3)

Remo Dietlicher[1], David Neubauer[1], and Ulrike Lohmann[1]

[1]Institute for Atmospheric and Climate Science, ETH Zürich, Universitätstrasse 16, 8092 Zürich, Switzerland.

Correspondence to: Remo Dietlicher (remo.dietlicher@env.ethz.ch)

Abstract. A new scheme for stratiform cloud microphysics has been implemented in the ECHAM6-HAM2 general circulation model. It features a widely used description of cloud water with two categories for cloud droplets and rain drops. The unique aspect of the scheme is the break with the traditional approach to describe cloud ice analogously. Here we parameterize cloud ice with a single, prognostic category as it has been done in regional models and most recently also in the global model CAM5. A single category does not rely on heuristic conversion rates from one category to another. At the same time it is conceptually easier and closer to first principles.

This work shows that a single category is a viable approach to describe cloud ice in climate models. Prognostic representation of sedimentation is achieved by a nested approach for sub-stepping the microphysics scheme. This yields good results in terms of numerical stability and accuracy as compared to simulations with high temporal resolution.

The improvement of the representation of cloud ice in ECHAM6-HAM2 is twofold. Not only are we getting rid of heuristic conversion rates but we also find that the prognostic treatment of sedimenting ice allows to unbiasedly represent the ice formation pathway from nucleation over growth by deposition and collisions to sedimentation.

1 Introduction

Clouds are the major source of uncertainty in current climate projections as assessed by the last IPCC report (Stocker et al., 2013). Apart from synoptic-scale low pressure systems, clouds are not resolved by the coarse spatial resolution used in climate models which necessitates a transfer from grid-box mean model-states over the sub-grid distribution of humidity down to the microphysical properties of clouds. The circumstances require heuristic methods to represent the average response of clouds to natural and anthropogenic forcing.

Over the last 50 years the level of sophistication of the transfer methods from resolved to parameterized scales has steadily increased. Kessler (1969) built a scheme based on a system of continuity equations for vapor, cloud and precipitation which assumed that clouds form as soon as grid-box mean supersaturation is established and precipitate proportionally to their mass. This idea was refined by the work of Sundqvist (1978) to account for sub-grid cloudiness by assuming an inhomogeneous distribution of moisture within a model grid-box. Later on, polydisperse cloud droplets were represented (Beheng, 1994) which was the first step towards the nowadays common transfer from grid-box mean quantities down to the particle scales by the assumption of particle size distributions in two moment schemes. Since then, a multitude of studies document the

Geosci. Model Dev. Discuss., https://doi.org/10.5194/gmd-2017-164
Manuscript under review for journal Geosci. Model Dev.
Discussion started: 14 August 2017

Geoscientific Model Development Discussions

progress in both the representation of sub-grid clouds (e.g. Tompkins (2002)) and the extension of schemes based on particle size distributions to ice (e.g. Seifert and Beheng (2006)).

Li et al. (2012) assessed the ability of climate models to represent the amount of ice in clouds with the last generation of climate models. They found that the globally averaged, annual mean ice water path differs by a factor of 2 to 10 among the selected models. While all of the models in their study are in radiative balance, they do so at the cost of a wide variety of cloud ice contents due to the large uncertainty in their radiative properties. At the same time, new studies (Tan and Storelvmo, 2016) suggest that the phase state of a cloud is decisive for its radiative properties and strongly impacts the equilibrium climate sensitivity (ECS) (Tan et al., 2016). Satellite observations show furthermore that the occurrence of ice and mixed-phase clouds are tightly linked to precipitation fields (Muelmenstaedt et al., 2015; Field and Heymsfield, 2015) which further reinforces the importance of accurately representing cloud ice in models.

The response of climate, and in particular clouds, to a warming world induced by increasing carbon dioxide emissions is a highly discussed topic in the climate research community (Hope, 2015; Bony et al., 2015; Stevens et al., 2016; Tan et al., 2016; Schneider et al., 2017). Following Tan et al. (2016) we focus on improving the representation of the supercooled liquid fraction in climate models and hence cloud ice in general. As has been laid out by the study of Li et al. (2012) there is a lot of room for improvement in this area.

Many climate models represent ice by predefining categories for a given particle characteristic, such as ice crystals, planar snow flakes or dense and spherical graupel and hail particles (Seifert and Beheng, 2006). Widely used categories for ice particles in models are in-cloud ice and falling snow. With the coarse resolution employed in climate models, these categories serve to distinguish between cloud ice and precipitation. This approach is motivated by the analogous treatment for cloud liquid water where cloud droplets are separated from rain drops. However, unlike for liquid water where there is a clear scale separation between condensational growth and growth by collision and coalescence, the criteria to divide ice into an in-cloud category and a precipitating category is not well defined. This classification therefore differs from model to model and, being weakly constrained, the associated conversion rates are often used as tuning parameters. The conversion from cloud ice to snow ranges from size threshold based descriptions (Morrison and Gettelman, 2008) to process based descriptions like accretion and riming rates (Murakami, 1990). Due to this heuristic partitioning, cloud ice parameterizations are associated with a large uncertainty.

New studies (Morrison and Milbrandt, 2015; Jensen and Harrington, 2015) introduce techniques to describe cloud ice in a more continuous fashion. Contrary to the common approach of representing ice as a composition of different particle types, they suggest to use a single category whose properties adjust smoothly to cloud conditions and formation history. This eliminates the need to parameterize weakly constrained conversion processes among categories.

Describing a hydrometeor species with a single category implies that the entire category, including a potentially fast-falling part, has to be treated prognostically. Since prognostic precipitation categories are becoming more and more popular in multi-category schemes as well (Gettelman and Morrison, 2015; Sant et al., 2015), many approaches exist to locally increase time resolution in order to achieve numeric stability. Here we adopt a multi-level sub-stepping approach to the ECHAM6-HAM2 general circulation model (GCM).

Geosci. Model Dev. Discuss., https://doi.org/10.5194/gmd-2017-164
Manuscript under review for journal Geosci. Model Dev.
Discussion started: 14 August 2017

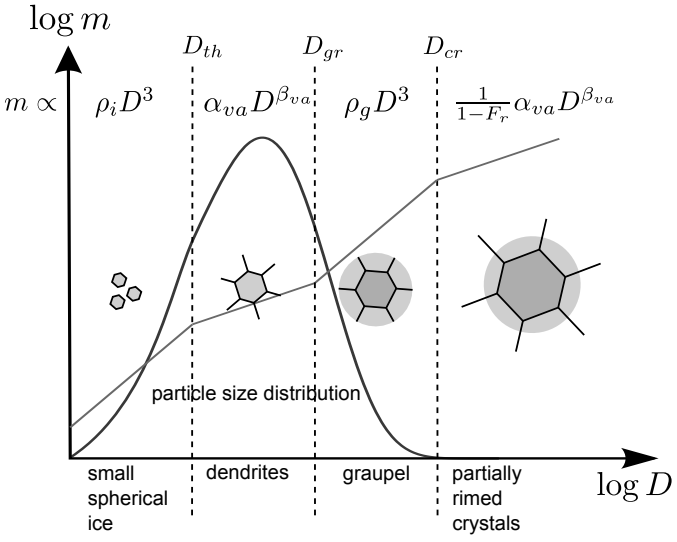

Figure 1. Summary of the mechanism used in the single category scheme. ρ_i is the density of ice, α_{va} and β_{va} are empirical constants, ρ_g is the diagnosed graupel density and $F_r = \frac{q_{rim}}{q_i}$ is the rime fraction.

In this study we focus on the pathways subsequent to ice initiation by a more physically-based description of cloud ice but acknowledge the importance of ongoing research to understand freezing mechanisms (Welti et al., 2014; Ickes et al., 2015; Marcolli, 2017) and resulting parameterization development (Phillips et al., 2013; Ickes et al., 2017). We will use the microphysical properties of ice described in Morrison and Milbrandt (2015) (hereafter MM15) and embed them in the ECHAM6-HAM2 microphysics scheme. A short summary of their scheme is given in Sect. 2. As this new approach leads to a revision of the existing cloud microphysics scheme, the entire scheme is described in Sect. 3. Numerical challenges associated with the prognostic treatment of sedimenting ice are addressed in Sect. 4. Section 5 shows the characteristics of the new microphysics scheme in a 1-D single column setup as well as an assessment of differences to the previous two category scheme. Section 6 concludes this study by evaluating the feasibility and benefit from using a single category ice phase scheme in the climate model ECHAM6-HAM2.

2 Revision of the single category scheme

A short review of the fundamental concepts of the single category scheme is given here. A detailed description of the scheme developed by MM15, also known as the predicted bulk particle properties scheme (P3), can be found in their paper.

Instead of the two categories for cloud ice and snow, the single category scheme uses four prognostic parameters describing a single category: the total ice mass mixing ratio q_i, total ice number concentration N_i, riming mass mixing ratio q_{rim} and riming volume b_{rim}. For the particle size distribution the gamma distribution

$$N(D) = N_0 D^{\mu(\lambda)} e^{-\lambda D} \tag{1}$$

Geosci. Model Dev. Discuss., https://doi.org/10.5194/gmd-2017-164
Manuscript under review for journal Geosci. Model Dev.
Discussion started: 14 August 2017

with the three free parameters N_0, μ and λ is chosen. An empirical relationship between μ and λ reduces the number of free parameters from three to two. Together with the mass to size relationship

$$m(D) = \alpha D^{\beta}, \tag{2}$$

for α and β depending on the growth regime governed by the transition parameters D_{gr}, the size separating dendritic and graupel geometries and D_{cr}, the size separating graupel and partially rimed crystal geometries, there are 4 unknowns which are computed from the 4 prognostic parameters. The $m(D)$ and $N(D)$ relationships together with the transition sizes are summarized in Fig. 1.

The basic idea of the scheme is to separate ice crystal growth by deposition from growth by collisions with cloud droplets that will increase the rime fraction of the ice bulk. While depositional growth is associated with $m(D) \propto D^3$ and therefore spherical particle geometry, growth by riming is associated with $m(D) \propto D^{\beta_{\mathrm{va}}}$ where $\beta_{\mathrm{va}} < 3$ assuming the predominant crystal has an oblate structure.

The weakly constrained parameters in the scheme are the α_{va} and β_{va} parameters in the $m(D)$ relation as well as the parameters describing the projected area $A(D)$ which is essential for the microphysical process rate calculations. The sensitivity to the involved parameter choices in the global context is elaborated in a recent publication by Eidhammer et al. (2017).

For this study we use the ice particle property lookup tables of the original P3 scheme.

3 Description of the cloud microphysics scheme

We developed a new cloud microphysics scheme in the framework of the ECHAM6-HAM2 (echam6.3.0-ham2.3-moz1.0) (Zhang et al., 2012; Stevens et al., 2013). The original cloud microphysics scheme solves prognostic equations for the mass mixing ratios of cloud liquid and ice (Lohmann and Roeckner, 1996). Snow and rain are diagnosed from the cloud mass mixing ratios of the respective phase. Over the years, this scheme was expanded to improve the representation of microphysical processes by adding prognostic equations for the number concentrations for cloud droplets and ice crystals (Lohmann et al., 1999; Lohmann, 2002). Conversion rates involving the ice phase date back to Lin et al. (1983) and Murakami (1990). The inclusion of a completely new approach to describe ice properties brought changes to many parameterizations and required a complete restructuring of the code to allow for sub-stepping. The following will describe the implementation of the microphysics scheme with a single category ice phase.

The snow category has been removed and instead, in addition to ice mass and number, the riming mass and riming volume are introduced to make up the four moment single category ice described in MM15. Except for the restructuring of the code explained in Sect. 3.1, the two category description of the liquid phase did not change. With the goal of better representing the supercooled liquid fraction, we changed the way the Wegener-Bergeron-Findeisen (WBF) process was parameterized. The original scheme did not allow deposition and condensation to occur simultaneously but parameterized the WBF process based on the sub-grid scale updraft velocity (Korolev and Mazin, 2003).

Geosci. Model Dev. Discuss., https://doi.org/10.5194/gmd-2017-164
Manuscript under review for journal Geosci. Model Dev.
Discussion started: 14 August 2017

3.1 Code structure

To better understand the model integration, consider a cloud parameter ϕ. This represents any of the prognostic parameters used in this scheme, e.g. cloud ice q_i or cloud liquid q_c. The model then solves the equation

$$\frac{\partial \phi}{\partial t} + \mathbf{u} \cdot \nabla \phi = \frac{\partial \phi}{\partial t}\Big|_{\mathrm{micro}} + \frac{\partial \phi}{\partial t}\Big|_{\mathrm{vdiff}} + \frac{\partial \phi}{\partial t}\Big|_{\mathrm{convection}} \tag{3}$$

where the left hand-side represents the resolved advection and the right hand-side the unresolved processes that need to be parameterized. The tendencies due to the microphysics routine are summarized here by $\partial\phi/\partial t\big|_{\mathrm{micro}}$. The tendencies $\partial\phi/\partial t\big|_{\mathrm{vdiff}}$ and $\partial\phi/\partial t\big|_{\mathrm{convection}}$ are calculated by ECHAM6-HAM2's vertical diffusion and convection modules (Stevens et al., 2013). Figure 2 shows how the microphysics tendency is further broken down in our implementation. The total rate of change by microphysical processes is split into the *grid-box mean* part describing the processes that only depend on the grid-box mean state of the model, the *in-cloud* part that represents below-cloud evaporation/sublimation and freezing/melting as well as collisional processes and *sedimentation* represents vertical transport of cloud ice. Therefore we write

$$\frac{\partial \phi}{\partial t}\Big|_{\mathrm{micro}} = \frac{\partial \phi}{\partial t}\Big|_{\mathrm{mean}} + \frac{\partial \phi}{\partial t}\Big|_{\mathrm{in-cloud}} + \frac{\partial \phi}{\partial t}\Big|_{\mathrm{sed}}. \tag{4}$$

The tendencies are given by

$$\begin{aligned}
\frac{\partial \phi}{\partial t}\Big|_{\mathrm{mean}} &= \frac{\partial \phi}{\partial t}\Big|_{\mathrm{tr}} + \frac{\partial \phi}{\partial t}\Big|_{\mathrm{ci}} + \frac{\partial \phi}{\partial t}\Big|_{\mathrm{act}} \\
\frac{\partial \phi}{\partial t}\Big|_{\mathrm{in-cloud}} &= \frac{\partial \phi}{\partial t}\Big|_{\mathrm{iaccl}} + \frac{\partial \phi}{\partial t}\Big|_{\mathrm{iacci}} + \frac{\partial \phi}{\partial t}\Big|_{\mathrm{raccc}} + \frac{\partial \phi}{\partial t}\Big|_{\mathrm{cautr}} + \frac{\partial \phi}{\partial t}\Big|_{\mathrm{e/s}} + \frac{\partial \phi}{\partial t}\Big|_{\mathrm{mlt}} + \frac{\partial \phi}{\partial t}\Big|_{\mathrm{frz}} \\
\frac{\partial \phi}{\partial t}\Big|_{\mathrm{sed}} &= \frac{\partial \phi}{\partial t}\Big|_{\mathrm{sedi}}
\end{aligned} \tag{5}$$

and the individual terms are discussed in detail below. The abbreviations in Eq. (5) stand for: *tr* cloud formation and dissipation by large-scale transport, *ci* nucleation and deposition in cirrus clouds allowing supersaturation with respect to ice, *act* activation of aerosols to cloud droplets, *mlt* melting of ice, *frz* homogenous and heterogeneous freezing, *iacci* accretion of ice by ice, *iaccl* accretion of liquid by ice, *e/s* below-cloud sublimation of rain and sedimenting ice, *cautr* and *raccc* the sedimentation sinks for liquid water by autoconversion and accretion of cloud droplets to rain, *sedi* sedimentation of ice.

Given the long time-step used for climate projections we split the computation in three parts, each of which is followed by an update of the local parameters. This allows condensation/deposition from large-scale convergence to be processed by the in-cloud and sedimentation calculations within a single time-step. Let ϕ^n be the state of the cloud parameter at time-step n. We calculate intermediate values

$$\begin{aligned}
\phi' &= \phi^n + \frac{\partial \phi^n}{\partial t}\Big|_{\mathrm{mean}} \Delta t, \\
\phi'' &= \phi' + \frac{\partial \phi'}{\partial t}\Big|_{\mathrm{in-cloud}} \Delta t, \\
\phi''' &= \phi'' + \frac{\partial \phi''}{\partial t}\Big|_{\mathrm{sed}} \Delta t
\end{aligned} \tag{6}$$

Geosci. Model Dev. Discuss., https://doi.org/10.5194/gmd-2017-164
Manuscript under review for journal Geosci. Model Dev.
Discussion started: 14 August 2017

Geoscientific Model Development Discussions

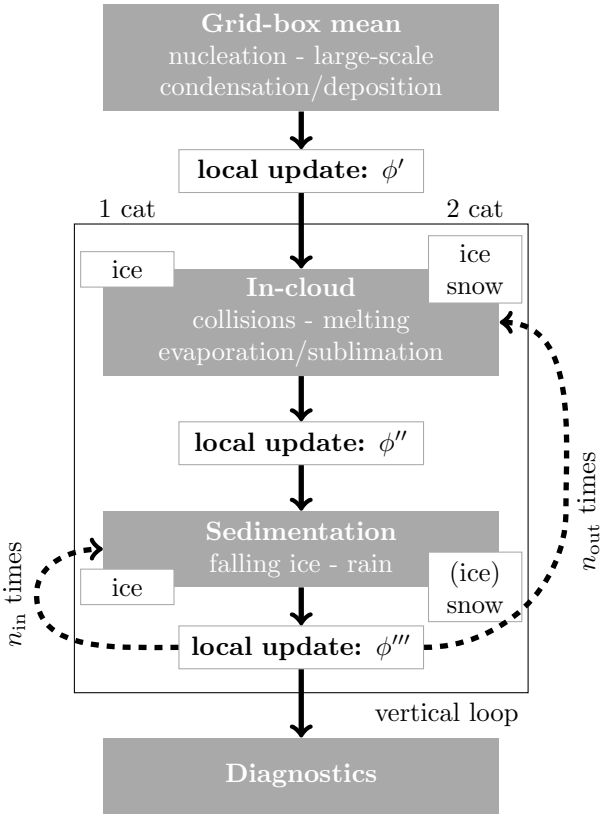

Figure 2. Flow diagram of the new scheme. The scheme is divided into 4 major parts: *Grid-box mean*, *in-cloud*, *sedimentation* and finally *diagnostics* after the process calculations. The model state is symbolized by ϕ as in the text. Boxes labeled *ice* and *snow* represent the ice hydrometeor types that are being handled in the new scheme on the left labeled *1 cat* and the old 2 category scheme labeled *2 cat* on the right. Dashed arrows represent the work-flow and sub-stepping. The box labeled *vertical loop* represents the part of the code that is looped vertically for the diagnostic treatment of rain. The parameters n_{in} and n_{out} refer to the number of time-steps in the inner and outer loop respectively.

and implement the total rate of change by microphysical processes (Eq. (4)) as the sum of the contributing terms

$$\left.\frac{\partial \phi^n}{\partial t}\right|_{\text{micro}} = \left.\frac{\partial \phi^n}{\partial t}\right|_{\text{mean}} + \left.\frac{\partial \phi'}{\partial t}\right|_{\text{in-cloud}} + \left.\frac{\partial \phi''}{\partial t}\right|_{\text{sed}}. \tag{7}$$

The process represented by Eq. (6) is visualized in the code structure diagram in Fig. 2 by the boxes labeled *local update*. In this notation we neglected the sub-stepping elaborated in Sect. 4 for clarity.

In the following subsections the parameterizations used to calculate the individual terms in Eq. (5) are presented.

Geosci. Model Dev. Discuss., https://doi.org/10.5194/gmd-2017-164
Manuscript under review for journal Geosci. Model Dev.
Discussion started: 14 August 2017

3.2 Grid-box mean processes

3.2.1 Cloud formation and dissipation

Condensation and deposition can occur before grid-box mean supersaturation is established. The formation and dissipation of a cloud depends on the convergence and divergence of relative humidity respectively (Sundqvist et al., 1989). The fractional cloud cover b is related to the relative humidity RH:

$$b = 1 - \sqrt{1 - \frac{\mathrm{RH} - \mathrm{RH}_c}{1 - \mathrm{RH}_c}} \tag{8}$$

where RH_c is a threshold grid-box mean relative humidity that has to be exceeded for cloud formation to be initiated. To cover the mixed-phase regime, we introduce a mixed-phase saturation specific humidity

$$q_s = f q_{s,l} + (1 - f) q_{s,i} \tag{9}$$

where f is a linear weighting function with $f(-35\,^\circ\mathrm{C}) = 0$ and $f(0\,^\circ\mathrm{C}) = 1$ and $q_{s,l/i}$ are the saturation specific humidities over liquid and ice. With that, RH is defined everywhere as $\mathrm{RH} = q/q_s$.

For all microphysics processes, b is used to calculate the in-cloud values, e.g. $q_i = \bar{q}_i/b$ where q_i is the variable used for in-cloud processes and $\bar{q}_i$ is the grid-box mean value.

Sedimenting ice and rain, which are allowed to fall into cloud free layers where $\mathrm{RH} < \mathrm{RH}_c$, use a sedimentation cover based on the cloud cover of the precipitating cloud. The sedimentation cover b_{sed} is simply diagnosed as the cloud cover at the base of the next cloud above.

The water mass Q that is available for condensation/deposition (or required to evaporate/sublimate) is given by

$$Q = -b(\Delta q_f - \Delta q_s) \tag{10}$$

where Δq_f is the moisture convergence in the grid-box by the resolved transport and Δq_s is the change in saturation specific humidity due to heat advection which includes the change given by the Clausius-Clapeyron equation as well as the temperature dependence of the weighting function $f(T)$.

We follow the approach of Morrison and Gettelman (2008) to directly include the WBF process in mixed-phase clouds and calculate the mass of water that is able to deposit on the existing ice crystals (Lohmann et al., 2016)

$$A = \Delta t N_i \alpha_m \frac{4\pi C(\mathrm{RH}_i - 1)}{F_k^i + F_d^i} \tag{11}$$

where $\alpha_m = 0.5$ is the probability of a water vapor molecule to successfully be incorporated into an ice crystal, Δt is the model time-step, $C = 2r_i/\pi$ is the capacitance of a planar ice particle and F_k^i and F_d^i are thermodynamic parameters depending only on temperature. It is assumed that $RH_i = q_{s,l}/q_{s,i}$ i.e. that the cloudy portion of the grid-box is at water saturation as long as liquid water is present in mixed-phase clouds. Additionally, it is assumed that ice crystal growth is prioritized over liquid droplet growth. With those two assumptions, the following rules determine the condensation and deposition in mixed-phase clouds.

Geosci. Model Dev. Discuss., https://doi.org/10.5194/gmd-2017-164
Manuscript under review for journal Geosci. Model Dev.
Discussion started: 14 August 2017

Geoscientific Model Development Discussions

In a cloud forming environment ($Q > 0$), the mass available for deposition is the sum of the excess water vapor Q and the liquid water q_c. If $Q < A$ the missing water is taken from the liquid phase and thus represents the WBF process. Otherwise both cloud droplets and ice crystals grow. In the case of a dissipating cloud ($Q < 0$), cloud droplets evaporate first and only if $q_c < Q$ ice crystals sublimate.

The growth and dissipation of pure ice clouds in the mixed-phase temperature regime ($0\,°\mathrm{C}$ to $-35\,°\mathrm{C}$) follows that dictated by Eq. (10) to be consistent with the cloud fraction in Eq. (8). Cirrus clouds are handled separately and are discussed in the next sub-section.

3.2.2 Cirrus clouds

Homogeneous freezing of solution droplets in cirrus clouds is considered. Starting at around $140\,\%$ RH with respect to ice, it is evident that the in-cloud deposition discussed in the previous sub-section is not suited to represent such clouds as this scheme does not allow supersaturation by design. To capture this effect we allow supersaturation with respect to ice and use the parameterization described in Kärcher and Lohmann (2002) based on sub-grid updraft velocity inferred from the turbulent kinetic energy to transfer from the grid-box mean state to a more physical sub-grid distribution of saturation values.

3.2.3 Aerosol activation

The model ECHAM6-HAM2 used in this study is equipped with the online aerosol model HAM version 2 (Zhang et al., 2012). Number concentrations and mass mixing ratios of 5 aerosol species (sulfate, sea salt, mineral dust, black carbon and organic carbon) are calculated with the aerosol module HAM. Aerosol activation is calculated according to Abdul-Razzak et al. (1998) and Abdul-Razzak and Ghan (2000) where the transition from grid-box mean to the physically relevant sub-grid formulation is done according to the sub-grid updraft velocity. We apply a correction to cloud droplet number concentrations if the mass-weighted mean droplet size is unphysically large because aerosol activation was too weak. For that, we adjust the number concentration such that a volume mean droplet radius of $25\,\mu\mathrm{m}$ is not exceeded.

3.3 In-cloud processes

3.3.1 Freezing of cloud droplets

The freezing capabilities of black carbon and mineral dust are calculated according to the parameterization developed by Lohmann and Diehl (2006). It accounts for both contact freezing of mineral dust and immersion freezing of black carbon and mineral dust in stratiform mixed-phase clouds.

3.3.2 Liquid-Ice interactions

Collisions between cloud droplets and ice crystals are calculated based on the ice particle's projected area and fall speed. These properties are part of the new single category description of ice and further described by MM15. The current diagnostic treatment of rain does not allow to calculate rain drop collection by ice on a physical basis. We assume that this process can

Geosci. Model Dev. Discuss., https://doi.org/10.5194/gmd-2017-164
Manuscript under review for journal Geosci. Model Dev.
Discussion started: 14 August 2017

be neglected and riming will be dominated by cloud droplets colliding with ice particles. This is equivalent to the original microphysics scheme in ECHAM6-HAM2.

3.3.3 Ice particle self-collection

With the size distribution and projected area to diameter relation intrinsic to the single category scheme we are able to numerically integrate the collection kernel. The resulting process rates are stored and read from lookup tables. This replaces the aggregation parameterization employed by the original scheme to calculate the efficiency with which ice crystals collide to form snow.

3.3.4 Below cloud evaporation/sublimation and melting

The evaporation of rain is calculated according to Rotstayn (1997). For ice we use the same formulation for below cloud sublimation as employed for deposition by moisture convergence (Eq. (11)) where we use the grid-box mean subsaturation with respect to ice. This implies that we neglect a potential subgrid distribution of humidity in completely cloud-free grid-boxes.

Melting is assumed to completely deplete cloud ice within one global time-step. Due to the variable time-step lengths owing to the sub-time-stepping described in Sect. 4 we assume a melting timescale of $\tau_{\mathrm{mlt}} = 1\,\mathrm{min}$ to assure complete melting to take place within a global time-step to be consistent with the original scheme.

3.4 Sedimentation

3.4.1 Cloud droplet autoconversion and accretion by rain

The sedimentation of liquid water is diagnosed by a separate category for rain that is assumed to fall through the whole column within one single global time-step. Rain is formed by autoconversion and increased by accretion. Autoconversion from cloud water to rain is calculated from the cloud liquid mass mixing ratio q_c and the number concentration of cloud droplets N_c following the empirical relation (Khairoutdinov and Kogan, 2000):

$$\left.\frac{\partial q_r}{\partial t}\right|_{\mathrm{aut}} = 1350 q_c^{2.47} N_c^{-1.79} \tag{12}$$

where q_r is the rain mass mixing ratio. Rain falling from above is also able to grow by accretion of cloud droplets following:

$$\left.\frac{\partial q_r}{\partial t}\right|_{\mathrm{acc}} = 3.7 q_c q_r \tag{13}$$

The rain flux is then given by (Stevens et al., 2013)

$$P_{\mathrm{rain}} = \frac{1}{g}\int_0^p (S_{\mathrm{aut}} + S_{\mathrm{acc}} + S_{\mathrm{mlt}} - S_{\mathrm{evp}})dp. \tag{14}$$

Geosci. Model Dev. Discuss., https://doi.org/10.5194/gmd-2017-164
Manuscript under review for journal Geosci. Model Dev.
Discussion started: 14 August 2017

Geoscientific Model Development Discussions

for pressure p and the source and sink terms of autoconversion from cloud droplets to rain $S_{\rm aut} = \frac{\partial q_r}{\partial t}\big|_{\rm aut}$, accretion of cloud droplets by rain $S_{\rm acc} = \frac{\partial q_r}{\partial t}\big|_{\rm aut}$, melting of ice $S_{\rm mlt}$ and evaporation of rain $S_{\rm evp}$. Given the precipitation velocity of rain, the rain mass mixing ratio q_r used for the accretion rate can be calculated from the rain flux $P_{\rm rain}$.

3.4.2 Falling ice

Sedimentation of ice is calculated prognostically according to MM15. The rate of change due to sedimentation is deduced from the number-weighted mean ($v_{\rm n}$) and mass-weighted mean ($v_{\rm m}$) fall speeds

$$v_{\rm n} = \frac{\int_0^\infty v(D)N(D)dD}{\int_0^\infty N(D)dD} \tag{15}$$

$$v_{\rm m} = \frac{\int_0^\infty v(D)m(D)N(D)dD}{\int_0^\infty m(D)N(D)dD}. \tag{16}$$

The fall speeds are computed offline and are read back from lookup tables.

The rate of change due to sedimentation is then simply given by

$$\frac{\partial X}{\partial t}\Big|_{\rm sed} = -\frac{v_{m/n}}{\Delta z}X \tag{17}$$

where X represents the ice moments: number- $n_{\rm i}$, ice- $q_{\rm i}$, rimed ice- $q_{\rm rim}$ and volume mixing ratio $b_{\rm rim}$. The number mixing ratio sediments according to the number-weighted mean fall speed $v_{\rm n}$, the other three according to the mass-weighted mean fall speed $v_{\rm m}$.

To mitigate instability due to a violation of the Courant-Friedrichs-Levy (CFL) criterion sub-stepping was applied to the relevant part. This will be further explained in Sect. 4.

4 Numerical aspects

The standard version of ECHAM6-HAM2 diagnoses precipitation assuming it reaches the surface within one global model time-step. Treating sedimentation prognostically requires much smaller model time-steps to resolve the vertical motion of hydrometeors by sedimentation. We therefore introduce sub-time-stepping in the microphysics and sedimentation calculations in order to achieve numeric stability as dictated by the CFL condition. For sedimentation we use the explicit Euler integration scheme. For this scheme, the CFL condition states that the CFL-number

$$\alpha(\Delta t) = v_m \Delta t/\Delta z \tag{18}$$

does not exceed unity in the whole domain for temporal and vertical resolutions Δt and Δz respectively. The length of the time-step is adjusted dynamically to ensure numerical stability. Furthermore note that we will always have $v_n < v_m$ since the averaging of v_m in Eq. (16) puts more weight to heavier and therefore faster falling particles. We assume that sedimenting ice

Geosci. Model Dev. Discuss., https://doi.org/10.5194/gmd-2017-164
Manuscript under review for journal Geosci. Model Dev.
Discussion started: 14 August 2017

cannot leave the grid-box column. Therefore the sedimentation domain is restricted to single columns. We will use $\alpha(\Delta t)$ in the following description to denote the maximal CFL-number within a given column for a time resolution Δt.

We apply a nested approach to increase the time resolution: an outer loop that comprises both microphysics and sedimentation as well as an inner loop for sedimentation only. A similar kind of multi-level sub-stepping is also used in e.g. Gettelman et al. (2015).

The inner loop is computationally very cheap and is therefore the main tool to keep the CFL-number of sedimentation $\alpha(\Delta t'')$ small, where $\Delta t''$ is the inner sub-time-step. We choose the number of time-steps n_{in} such that $\alpha(\Delta t'') \ll 1$ for $\Delta t'' = \Delta t'/n_{in}$ for the outer sub-time-step $\Delta t'$. We found reasonable convergence for a rather weak restriction of $\alpha(\Delta t'') < 0.25$.

The outer loop is more expensive and comprises all the microphysical parameterizations. Just as with the inner loop, we choose n_{out} such that $\alpha(\Delta t') \leq 1$ where now $\Delta t' = \Delta t/n_{out}$ for the global time-step Δt. Since we want to have the microphysics scheme acting on falling ice at least once per vertical layer, we require $\alpha(\Delta t') \sim 1$.

The sub-stepping workflow is shown by the dashed arrows in Fig. 2. Here the nested aspect of the sub-stepping becomes clear. For every one of the n_{out} iterations of the outer loop, the inner loop is called n_{in} times. Together they ensure numerical stability and allow to represent the advection of falling ice to be done reasonably well with the simple Euler method.

Note that only grid-boxes where temperature is below $0\,°\mathrm{C}$ have to be considered in the online calculation of n_{in} and n_{out}. In practice we loosen the requirement to an upper temperature limit of $5\,°\mathrm{C}$ since there is a finite timescale associated with melting and therefore very fast falling hydrometeors may still reach regions above $0\,°\mathrm{C}$. The restriction to cold temperatures significantly reduces the number of iterations since the low temperatures allowing for ice to form are most commonly found in high altitudes where the model has a coarse vertical resolution i.e. Δz is large and α is consequently small.

To demonstrate the need to apply the sub-stepping described above, we employ a simple single column setup with 31 vertical levels. At one single model level at around $400\,\mathrm{hPa}$ a constant ice source term with specified tendencies for all 4 ice moments is prescribed at every time-step. The temperature profile is prescribed, constant in time and set to the international standard atmosphere ($15\,°\mathrm{C}$ at the ground decreasing linearly with height to reach $-40\,°\mathrm{C}$ at $400\,\mathrm{hPa}$). The microphysical processes are restricted to sedimentation and melting. Representing the melting layer is a good test to disentangle the effect of the inner and outer sub-stepping loops. The resulting ice profile undergoes a build-up phase until it reaches the equilibrium where the source term is balanced by the precipitation sink.

Results from this idealized experiment are shown in Fig. 3 and Fig. 4. Since we are investigating numerical errors due to insufficient time resolution, the high-resolution run (*T6*; black, dashed line) with a time-step of $6\,\mathrm{s}$ may be regarded as the truth in the following analysis. We did not change the vertical resolution, therefore CFL-numbers $\alpha(6\,\mathrm{s})$ are very small throughout the column and no sub-stepping needs to be applied in the *T6* case.

A violation of the CFL-criterion leads an artificial slowdown of sedimentation. The simulation without sub-stepping (*NO*) confirmingly shows a clear delay in surface precipitation onset, cf. Fig. 3b. This onset delay leads to an accumulation of ice in the atmosphere, even though eventually the same precipitation rate is reached once an equilibrium between the humidity input and the sedimentation sink has been established.

Geosci. Model Dev. Discuss., https://doi.org/10.5194/gmd-2017-164
Manuscript under review for journal Geosci. Model Dev.
Discussion started: 14 August 2017

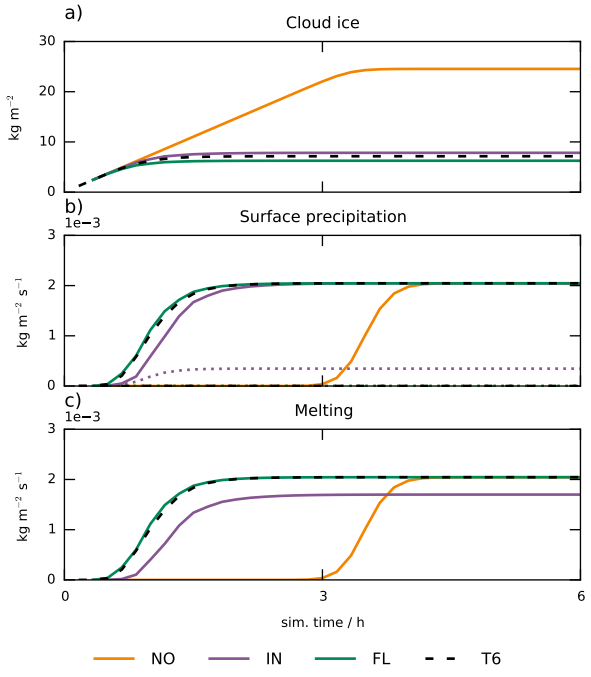

Figure 3. Results from a simple throughput experiment in the single column model. The sub-figures show cloud ice (a), surface precipitation (b), part of which is the snowfall rate (dotted lines in (b)), and vertically integrated melting rates (c). Colors indicate different simulation setups: T6 uses a time-step of 6 s. In the simulations FL, IN and NO a global time-step of 600 s is used. They differ in their sub-stepping: FL has full sub-stepping with online computation of n_{in} and n_{out}, IN sets $n_{out} = 1$ and only uses the inner loop with online computation of n_{in} and NO does not use any sub-stepping with constant $n_{in} = n_{out} = 1$.

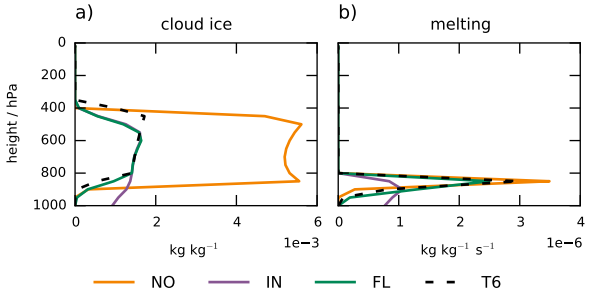

Figure 4. As in Fig. 3 but for vertical profiles at equilibrium, evaluated after 12 h of the simulation.

Geosci. Model Dev. Discuss., https://doi.org/10.5194/gmd-2017-164
Manuscript under review for journal Geosci. Model Dev.
Discussion started: 14 August 2017

Geoscientific Model Development Discussions

The significance of the outer loop is demonstrated by the vertical profiles at equilibrium. If we allow $\alpha(\Delta t') > 1$ but restrict $\alpha(\Delta t'') < 0.25$, ice might pass a grid-box without having the microphysical processes acting on it. This out of sync effect leads to the ice mass profile (*IN*) shown in Fig. 4a. Melting can not take place because microphysics is not called, leading to non-zero cloud ice at temperatures well above $0\,°\mathrm{C}$ and significant snow fall rates, cf. Fig. 3b.

There still is an error in the representation of the melting layer in the simulation with full sub-stepping (*FL*) leading to a small spread of the melting rate towards higher temperatures. This is the price for the efficiency gained by reducing the CFL-number with the cheap inner loop without calling the microphysics every sub-step.

4.1 Sub-stepping and the diagnostic treatment of rain

This section provides a closer look at the rain flux within the sub-stepping environment. A diagnostic treatment of precipitation is designed for very large time-steps where the vertical movement of rain drops cannot be resolved. Since the new scheme in principle allows to resolve falling hail particles, we are outside of the realm the rain flux scheme was originally designed for. Since this work focuses on the representation of cloud ice, we will not discuss potential improvements to the liquid phase that would benefit from the already employed sub-stepping. The obvious improvement would be making it prognostic all together as was done by Sant et al. (2013). Sticking with the rain flux approach, it is important to rule out any systematic biases of rain production associated with the sub-stepping employed for cloud ice.

To estimate the sensitivity of rain production on the number of sub-steps, we use a similar setup as for the ice sedimentation: A single column simulation with an isothermal atmosphere at $20\,°\mathrm{C}$ and a relative humidity of $100\,\%$ throughout the column. A humidity tendency of $5 \times 10^{-7}\,\mathrm{kg\,kg^{-1}\,s^{-1}}$ is applied to the model levels between 16 and 26 (corresponding to $400\,\mathrm{hPa}$ to $900\,\mathrm{hPa}$ in pressure levels). This forcing is representative of a stratiform cloud formation in the global setup of the model and corresponds to a water column tendency of $2\,\mathrm{mm\,h^{-1}}$. For this experiment we fixed the cloud droplet number concentrations but vary their (constant) values from $50\,\mathrm{cm^{-3}}$ to $500\,\mathrm{cm^{-3}}$ to represent clouds with stronger and weaker rain production rates.

The simulations are run for one day with the humidity forcing active throughout the whole simulation. Every simulation is run once with $n_{out} = 1$, i.e. without sub-stepping affecting rain production and once with $n_{out} = 100$, i.e. with a very large number of sub-steps. Figure 5 shows the vertically integrated rain production rate together with its constituents: rain enhancement by accretion of cloud droplets by rain drops and autoconversion of cloud droplets to rain drops.

The first row in Fig. 5 indicates that different numbers of sub-steps and thus different time-step lengths can lead to relative differences in the rain production rate of up to $25\,\%$ for the simulations with the lowest number concentrations and therefore strongest rain production rates. The relative difference decreases to below $10\,\%$ for weaker rain production rates. Eventually, every simulation reaches an equilibrium where the humidity input is balanced by the rain sink. This external constraint leads to vanishing differences in equilibrium rain production rates for different numbers of sub-steps. The second and third rows show the constituents of the total rain production rate. These rates show that there is no compensation of errors by the accretion and autoconversion rates but rather that the differences are due to the overestimation of precipitation production by the linearized numerical integration method employed by the core model. The local update of q_c and N_c by sub-stepping Eq. (12) and Eq. (13) reduces the numerical error of the accretion and autoconversion rates and prevents the overshooting of precipitation formation

Geosci. Model Dev. Discuss., https://doi.org/10.5194/gmd-2017-164
Manuscript under review for journal Geosci. Model Dev.
Discussion started: 14 August 2017

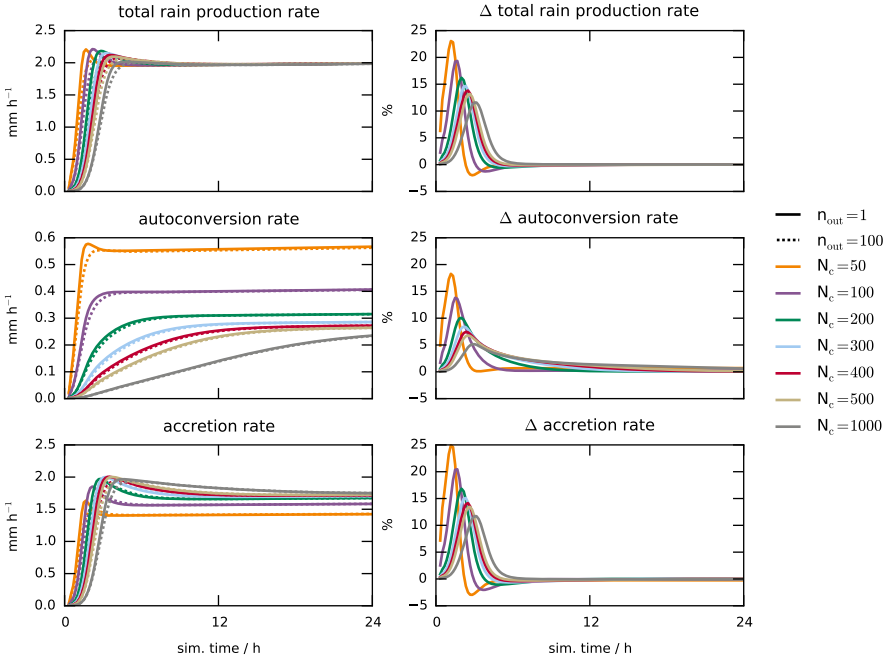

Figure 5. Rain production rates for the simulations described in the text. Solid lines are simulations with $n_{out} = 1$ and dashed lines are simulations with $n_{out} = 100$. Different colors represent simulations with different cloud droplet number concentrations reaching from $50\,\mathrm{cm}^{-3}$ to $1000\,\mathrm{cm}^{-3}$. The left column shows the total rain production rate and its constituents autoconversion of cloud droplets to rain drops and accretion of cloud droplets by rain drops. The right column shows the relative differences ($(R^1 - R^{100})/R^1$, for R^n being any of the rates above) between the simulations with $n_{out} = 1$ and $n_{out} = 100$ for every process.

that can be seen in the $n_{out} = 1$ simulations. This claim is backed up by a simulation with high temporal resolution which is almost identical to the simulation with 100 sub-steps and therefore not shown. We conclude that sub-stepping is beneficial for the representation of the rain flux.

Varying the number of outer time-steps from 1 to 100 is an extreme case. In the global model setup the number of outer sub-steps ranges on average from 5 in the tropics to 25 in mid-latitudes. Since the model converges quickly with increasing number of time-steps, the differences of 10 % to 25 % represent an upper boundary. We conclude that for our purpose a diagnostic scheme for liquid water is compatible with the prognostic treatment of cloud ice and no significant systematic biases are induced by the number of sub-steps used. This is important as the number of sub-steps is computed online and may vary between columns.

Geosci. Model Dev. Discuss., https://doi.org/10.5194/gmd-2017-164
Manuscript under review for journal Geosci. Model Dev.
Discussion started: 14 August 2017

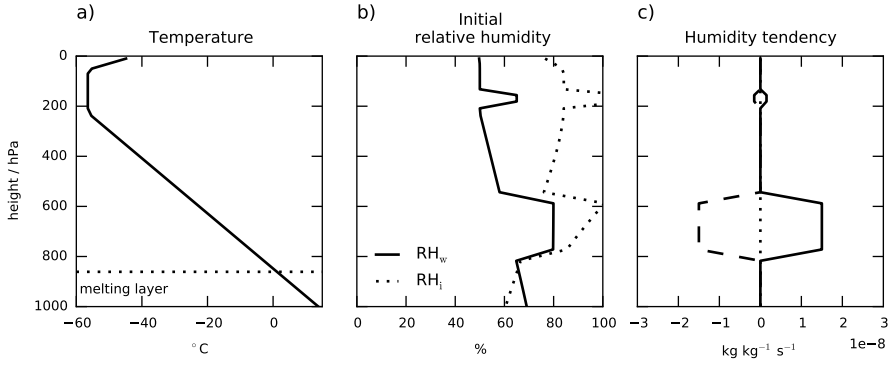

Figure 6. Vertical profiles of the single column model column initial conditions and forcing terms. Temperature is initially set to the international standard atmosphere temperature profile (a) with a humidity profile allowing for cloudy regions (b) in cirrus and mixed-phase regimes. A humidity forcing is applied to initiate cloud formation (c). Solid lines show the forcing during cloud formation, dotted lines show the stable phase without forcing and the dashed lines show the dissipation forcing.

5 Results

To demonstrate the behavior of the new scheme we look at results from a more elaborate single column simulation than the one used in Sect. 4. The setup is summarized by the initial and forcing profiles shown in Fig. 6. It allows for an isolated view on the microphysics scheme by deactivating the convection, vertical diffusion and radiation parameterizations and allowing no surface evaporation. Initial conditions are set to the international standard atmosphere with two cloudy regions: One in the cirrus and one in the mixed-phase regime (Fig. 6a and b). We run the simulations for $36\,\mathrm{h}$. For the first $12\,\mathrm{h}$ a humidity tendency is applied to the cloudy regions (solid lines in Fig. 6c). For the last $12\,\mathrm{h}$, tendencies equal in magnitude but with opposite sign (dashed lines in Fig. 6c) are applied such that the total water content is the same for simulation times $0\,\mathrm{h}$ and $36\,\mathrm{h}$. In between the formation and dissipation phases there is a $12\,\mathrm{h}$ stable phase without humidity forcing. The temperature is kept constant throughout the simulation to compensate for latent heating by condensation/evaporation and deposition/sublimation. Since the vertical diffusion and convection parameterizations are turned off this assures that the melting layer remains at the same level throughout the simulation which facilitates the interpretation of the results.

We prescribe mineral dust and sulfate aerosols which dominate heterogeneous freezing in mixed-phase conditions and homogeneous nucleation in cirrus clouds respectively. Cloud droplet number concentration is fixed at a constant value representative of marine clouds of $100\,\mathrm{cm}^{-3}$ since we are mainly interested in the evolution of cloud ice.

5.1 Comparison to the original scheme

The standard version of ECHAM6-HAM2 is equipped with a 2 moment scheme for both cloud liquid water and ice and diagnostic equations for snow and rain mass mixing ratios. For comparability, the new scheme can switch between calculating in-cloud and sedimentation tendencies based on the new single category and the original two category scheme. This way we

Geosci. Model Dev. Discuss., https://doi.org/10.5194/gmd-2017-164
Manuscript under review for journal Geosci. Model Dev.
Discussion started: 14 August 2017

Geoscientific Model Development Discussions

	1 category scheme	*2 category scheme*	*2.5 category scheme*
IC properties	P3	P3 (dendrites)	P3 (dendrites)
IC sedimentation type	prognostic	off	diagnostic
IC sedimentation scheme	P3	-	Rotstayn (1997)
Diagnostic snow	-	Murakami (1990)	Murakami (1990)

Table 1. Summary of the ice description for the three schemes mentioned in the text. Ice crystals are abbreviated by *IC*. P3 represents a description of particle properties according to Sect. 2. Since this analysis is focused on the different cloud ice schemes (prognostic single category vs. diagnostic two category) we use the P3 properties for ice crystals also in the 2 and 2.5 category schemes, assuring comparable fall speeds and deposition rates. Since those schemes only consider riming for snow, P3 is reduced to pure dendritic particles (i.e. $F_r = 0 \Leftrightarrow D_{gr} = D_{cr}$).

are able to consider only the differences between the schemes that are due to the conversion of cloud ice to snow in the original scheme and the single category approach while all grid-box mean and the compatible in-cloud (melting of in-cloud ice and freezing) computations are identical. The parts in the code where this switch affects the simulation are shown by the *ice* and *snow* tags in the code flowchart in Fig. 2. The tags on the left represent ice in the single category and the tags on the right represent the two ice categories from the original scheme. *Ice* represents the in-cloud mass mixing ratio of ice in both schemes and *snow* is the diagnosed, precipitating category in the two category scheme.

Originally the two category approach was designed to separate fast falling hydrometeors, reaching the ground within one time-step, from those that stay in the cloud, i.e. those with effectively zero fall velocity. For cloud ice there is no unambiguous way to make this distinction. Therefore the original scheme in ECHAM6-HAM2 allows ice in the in-cloud category to fall as well (Lohmann et al., 2008). The vertical transport of ice is based on the ice mass flux divergence of falling ice (Rotstayn, 1997). In regions without cloud ice the ice mass flux diminishes exponentially with height and is only subject to sublimation and melting.

In Fig. 7 and Fig. 8 the results from simulations using the single category and the original scheme are shown. In order to investigate the processes in mixed-phase clouds, the formation of cirrus clouds shown in Fig. 6 is turned off. We show two versions of the original scheme: The conventional two category scheme that separates falling snow from ice crystals, denoted as *2 category scheme*, and the scheme including the sedimentation of ice crystals with the ice mass flux divergence, denoted as *2.5 category scheme*. The 2.5 category scheme is the scheme used in the original cloud microphysics scheme of ECHAM6-HAM2. This notation reflects the fact that falling ice is only subject to melting and sublimation and all other microphysical processes are neglected. Therefore the treatment of falling ice crystals resembles a separate category. The cloud ice schemes for each simulation used in this section are summarized in Table 1.

In the *2 category scheme* simulation cloud ice is not allowed to fall. In the single column model ice crystals are therefore restricted to the level they formed in, which are the levels where heterogeneous freezing takes place. Since temperature decreases with height in the cloud this process is most active at cloud top, c.f. Fig. 7a. As soon as sufficient ice crystals have been formed, their accumulated depositional growth is able to quickly deplete the co-existing liquid water. The large mass transfer

Geosci. Model Dev. Discuss., https://doi.org/10.5194/gmd-2017-164
Manuscript under review for journal Geosci. Model Dev.
Discussion started: 14 August 2017

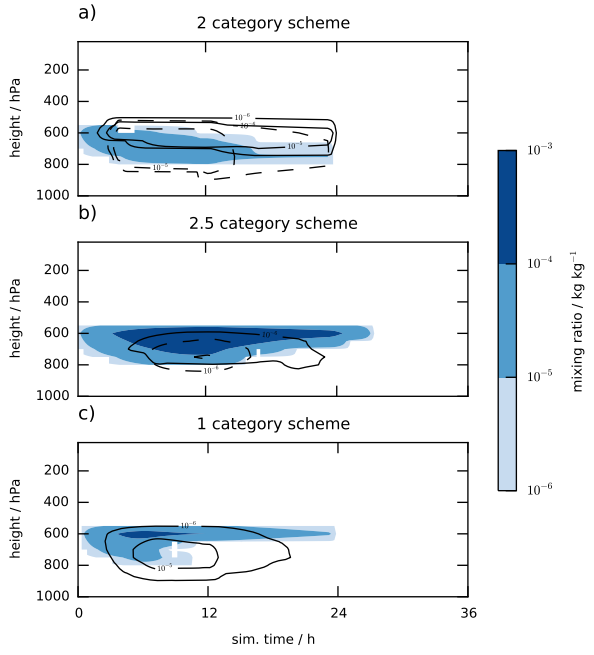

Figure 7. Timeseries of the vertical profiles of in-cloud ice (contour lines) and liquid water contents (colors). For the two category schemes snow mass is indicated by dashed lines. Note that snow is a vertically integrated quantity and the profile therefore is only an approximation. The sub-figures (a) and (b) show two versions the original scheme with diagnostic treatment of sedimentation as discussed in the text and sub-figure (c) shows the single category with prognostic ice sedimentation.

from the liquid to the ice phase grows the ice crystals to sizes where conversion to snow is efficient. Those snow particles partly deplete the liquid cloud below the freezing levels by riming and subsequently sublimate. The sublimation rate for snow is stronger than in the single category scheme such that most snow is sublimated before it reaches the melting level, see Fig. 8a and b. Snow is treated diagnostically and only the snow mass flux is calculated (Murakami, 1990). As such neither snow flake size nor fall speed are calculated on a physical basis. Consequently the sublimation rate cannot be calculated explicitely but is based on empiric relations (Lin et al., 1983).

The results from the *2.5 category scheme* simulation show how the situation changes when the ice crystals themselves are allowed to fall. The ice crystals that formed at cloud top do not accumulate in the levels of formation but spread throughout the cloud, see Fig. 7b. An exponential tail of the ice crystal mass flux continually falls out of the cloud where it sublimates. This steady removal of cloud ice does not allow the ice crystals to grow by vapor deposition and hence the snow production rate is weak. The riming rate is significantly reduced since the original scheme only considers collisions between snow flakes and cloud droplets as shown in Fig. 8c. The small riming and deposition rates lead to a mixed-phase cloud that is heavily dominated by liquid water. It is important to note that apart from very small snow production rate, this simulation only differs from the *1 category scheme* simulation by the diagnostic vs. prognostic treatment of ice crystal sedimentation. The challenge of treating

Geosci. Model Dev. Discuss., https://doi.org/10.5194/gmd-2017-164
Manuscript under review for journal Geosci. Model Dev.
Discussion started: 14 August 2017

Geoscientific Model Development Discussions

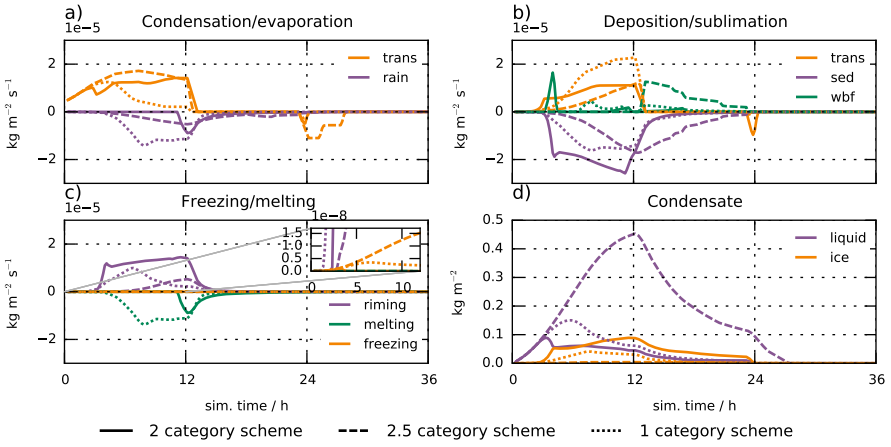

Figure 8. Timeseries for the vertically integrated phase change process rates for the simulations described in the text. The solid lines show results from the 2 category scheme with diagnostic snow, the dashed lines show results from the 2.5 category scheme with diagnostic snow and falling ice and the dotted lines show the results from the single category scheme with prognostic ice sedimentation. The sub-figures (a)-(c) show the rates of phase changes, (d) shows the vertically integrated condensate. Condensation and deposition rates are divided into changes due to by *trans*port (forcing term), evaporation of *rain* and sublimation of *sed*imenting ice. Ice growth at the expense of liquid is denoted by *wbf*.

the sedimentation of ice crystals diagnostically has been discussed in Rotstayn (1997). Our results support the hypothesis that a diagnostic scheme likely overestimates sedimentation.

The *1 category scheme* allows particles to grow by riming and vapor deposition at the same time. Given the initial conditions and forcing profiles in Fig. 6 and the available water Q defined in Eq. (10) one easily sees that Q increases with height. At cloud top, this allows cloud droplets and ice crystals to grow simultaneously (i.e. $A < Q$). Further down in the cloud where Q is smaller and the ice crystals are larger, thus growing more efficiently by vapor deposition, the WBF process is triggered (i.e. $A > Q$) and cloud liquid water diminishes over time. In the stable phase without humidity forcing (i.e. $Q = 0$) ice crystals grow at the expense of evaporating cloud droplets. However, the crystals that were small enough to stay at cloud top are too small to deplete the co-existing liquid water, leaving behind a liquid layer that evaporates in the cloud dissipation phase.

The analysis of the two versions of the original scheme highlights an important feature of diagnostic multi-category schemes. If one or multiple categories only consider a subset of the microphysical process rates, the conversion rates among those categories influence the relative strength of the associated process rates. In the simulations shown here we saw that the riming rate was significantly reduced by the employment of the ice mass flux divergence scheme. One could imagine a scheme that underestimates the sedimentation of ice crystals and uses another conversion rate from ice crystals to snow that results in a stronger snow production rate. This scheme will feature yet another combination of riming and vapor deposition rates and consequently another supercooled liquid fraction. The single category scheme with the prognostic sedimentation discussed in Sect. 4 does not have to distinguish between snow and ice crystals. The sedimentation of ice is resolved by the locally

Geosci. Model Dev. Discuss., https://doi.org/10.5194/gmd-2017-164
Manuscript under review for journal Geosci. Model Dev.
Discussion started: 14 August 2017

reduced time-step which allows the full set of microphysical parameterizations to be performed on the whole ice bulk. In mixed-phase clouds, this allows the riming, deposition and sedimentation processes to compete. As a result, the phase-state of the mixed-phase cloud is inferred on the physical basis of the parameterizations. Therefore a single category does not have the bias inherent to any multi category scheme that relies on a heuristic separation of cloud ice into different categories with predefined properties and maybe even different microphysical behavior (as is the case for our original scheme).

5.2 The rime fraction

The rime variables in the single category scheme, i.e. the rimed ice mass and the rimed ice volume, determine the density and shape of the particles with heavily rimed particles being spherical and weakly rimed particles having dendritic geometry. As a result, particles with high rime fractions have a smaller projected area and thus a higher fall speed than their weakly rimed counterparts of the same mass. Morrison and Milbrandt (2015) showed in a regional model that this adjustment of particle properties is crucial to correctly predict precipitation rates in a squall line simulation with strong convective updraft.

The ECHAM6-HAM2 GCM does not resolve those strong convective updrafts but parameterizes convection by the Tiedtke (1989) scheme. In its standard version, it employs very simplified microphysics which do not account for the co-existence of liquid water and ice. It is therefore questionable whether riming as such, and the resulting change in particle properties especially, is currently adequately represented in convective clouds.

From a purely stratiform cloud perspective, the effect of the particle properties on process rates is best illustrated by a seeder-feeder situation where ice crystals from a cirrus cloud precipitate through a liquid cloud. This section will explore this special case and shed light on the particle properties within the P3 parameterization.

Again we employ the setup summarized by the profiles in Fig. 6. The simulations are done with the new single category scheme. To investigate the sensitivity to the particle properties within this scheme, we change the effect of riming on the mass to size relationship of the P3 scheme described in Sect. 2. Two simulations are done: The *rime properties* simulation uses the regular particle properties of the P3 scheme and the *dendritic properties* simulation neglects the effect of riming on the mass to size relationship. With the notation from Sect. 2 this can be expressed by setting the rime fraction $F_r = 0$ which results in $D_{gr} = D_{cr}$. The only remaining transition parameter then is $D_{th} \equiv const$, separating the small spherical ice regime from the dendritic growth regime.

Fig. 9 shows a summary of the process rates and column integrated water masses for the vertical cloud profiles shown in Fig. 10a and d. We first remark that the ice mass generated by the cirrus cloud is about an order of magnitude smaller than the supercooled liquid cloud from Fig. 9d. From the same figure we can also see that neglecting the impact of riming on particle properties changes the thickness of the liquid cloud by roughly $10\,\%$. This can be attributed to the different riming rates in the two simulations.

Fig. 10 shows the particle properties for the two simulations. While the particles from the *rime properties* simulation get more dense by riming and their fall speeds increase up to almost threefold upon impact with the liquid cloud, the particles from the *dendritic properties* simulation do not factor in the rime fraction for the fall velocity calculation. Therefore these particles are less dense and fall more slowly which leads to a net increase in riming strength and duration.

Geosci. Model Dev. Discuss., https://doi.org/10.5194/gmd-2017-164
Manuscript under review for journal Geosci. Model Dev.
Discussion started: 14 August 2017

Geoscientific Model Development Discussions

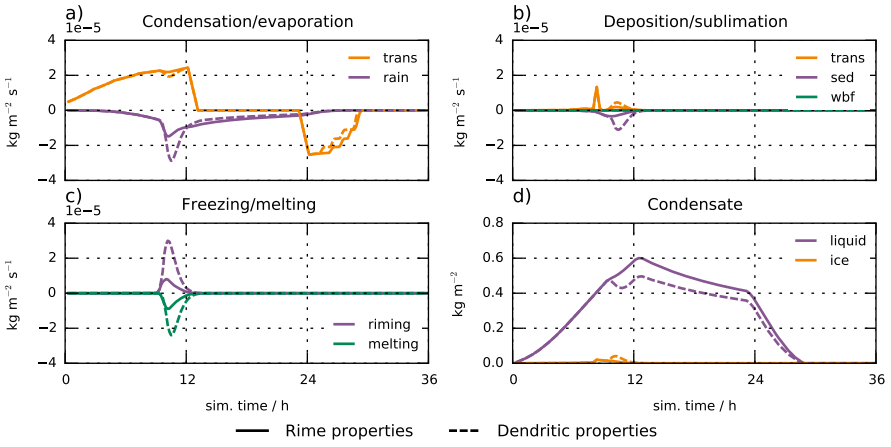

Figure 9. Same as in Fig. 8 but for simulations with the single category scheme where freezing in the mixed-phase cloud is turned off and the humidity forcing in the cirrus regime is turned on. The solid lines represent a simulation where riming affects the particle properties and the dashed lines represent a simulation where the mass to size relation for dendrites is assumed for all particles with diameter $D > D_{th}$.

Another noteworthy point is the fact that only the *dendritic properties* simulation shows significant below cloud sublimation. This is a manifestation of the prognostic treatment of cloud ice sedimentation. Since the vertical motion of the particles is resolved, the time available for the particles to sublimate is assessed on a physical basis. Therefore the fast-falling particles from the *rime properties* simulation do not undergo significant sublimation (Fig. 9b). The slower particles from the *dendritic properties* simulation on the other hand sublimate much stronger.

The idealized, purely stratiform and turbulence-free simulations shown here indicate that the influence of riming on the particle properties can alter the microphysical process rates substantially in this specific case with a very pronounced transition from dendritic to graupel-like properties.

5.3 A single category

The single category scheme is able to represent a wide range of particle properties representing small in-cloud ice crystals, larger dendrites and fast falling structures like graupel and hail.

It is important to remember, that the particle properties are parametrized by the particle size distribution, mass to size and mass to projected area relationships. Therefore a predefined relationship between the four prognostic ice parameters and the particle properties exists, which is layed out in Sect. 2. We would like to stress the fact that it is the four ice parameters that are prognostic and not the particle properties themselves.

This section provides a closer look at this pecularity of a single category scheme. We use a similar seeder-feeder simulation as in the last section but with a mixed-phase cloud instead of a pure liquid cloud as the feeder cloud. We will focus on three particular areas in the simulation, shown in Fig. 11a: 1) the mixed-phase cloud just before the cirrus particles impact (purple

Geosci. Model Dev. Discuss., https://doi.org/10.5194/gmd-2017-164
Manuscript under review for journal Geosci. Model Dev.
Discussion started: 14 August 2017

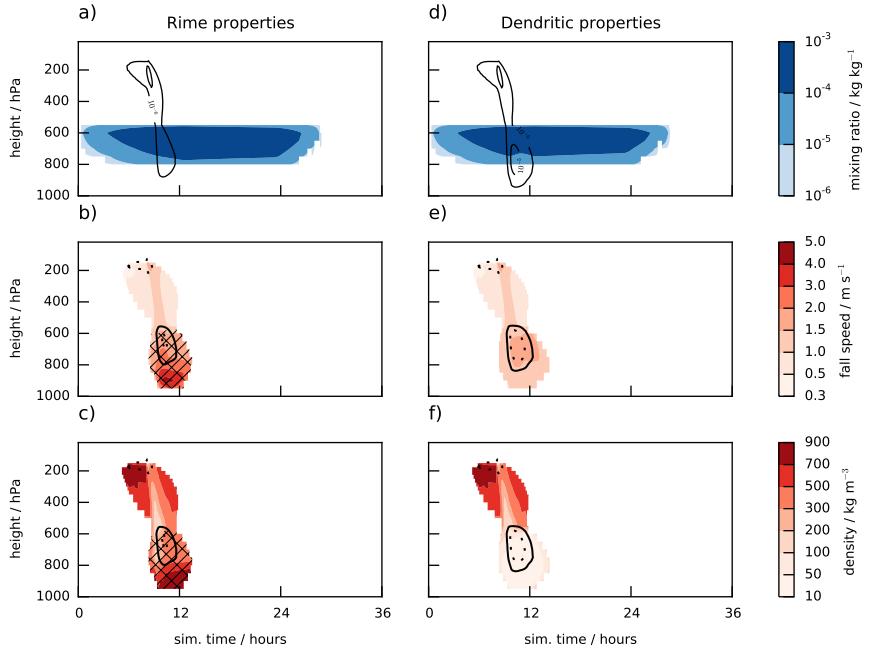

Figure 10. Timeseries of the vertical profiles of the particle properties for the seeder-feeder simulation described in the text. Figures a) to c) and d) to f) show results for the simulations with and without taking the change in particle properties due to riming into account respectively. Figures a) and d) show the water mixing ratios (colors for liquid, contours for ice), b) and e) show ice particle fall speeds and c) and f) show ice particle density. In figures b), c), d) and f) the solid and dotted lines show regions of significant ($> 10^{-9}\,\mathrm{kg\,kg^{-1}\,s^{-1}}$) riming and depositional growth respectively. Hatches mark areas where $F_r > 0.5$, i.e. where particles are dominated by rimed ice.

rectangle), 2) the cirrus particles just above the mixed-phase cloud (green rectangle) and 3) the resulting particles after impact (orange rectangle).

From the corresponding particle size distributions in Fig. 11b we can see how a single category handles the addition of two ice masses with differing particle properties. The tail of very large particles from the cirrus cloud is lost by averaging even though it contributes around $10\,\%$ to the total mass mixing ratio. This is because the total number concentration is heavily dominated by the mixed-phase cloud with the cirrus cloud only making up a small fraction of about $0.5\,\%$ thereof. Since the microphysical process rates are calculated from the resulting particle size distribution, particle collisions and the sedimentation sink are likely underestimated.

A solution to this issue has been proposed by Milbrandt and Morrison (2016) to use multiple free categories. Ice of different origin will then be sorted according to its diagnosed properties and stored in separate variables, thus giving the properties themselves a prognostic flavour. However, adding prognostic variables for multiple free categories is computationally expensive. We argue that in the context of climate projections where we are interested in global and regional mean states of the atmosphere,

Geosci. Model Dev. Discuss., https://doi.org/10.5194/gmd-2017-164
Manuscript under review for journal Geosci. Model Dev.
Discussion started: 14 August 2017

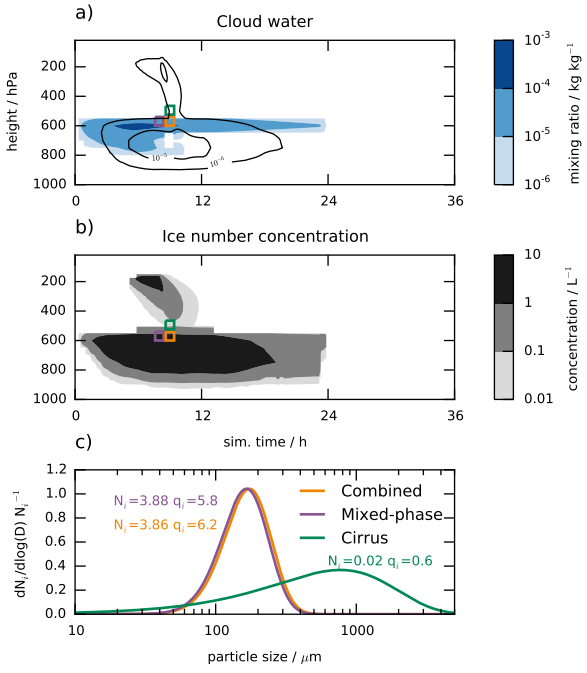

Figure 11. Timeseries of the vertical profile of water contents for the cirrus cloud above a mixed-phase cloud simulation described in the text are shown in sub-figure a) (black solid lines: ice, colors: liquid water). Sub-figure b) shows the same for the ice crystal number concentration. The rectangles in sub-figures a) and b) visualize the regions representative of the particle size distributions in sub-figure c) (not drawn to scale). Normalized particle size distributions for the rectangular areas in a) and b) are shown in sub-figure c). The purple and green lines represent the mixed-phase and cirrus particles before impact and the orange line is the combination of the two after impact. Since the size distribution is normalized we give the total number N_i for each distribution in the corresponding color in units of $1\,\mathrm{L}^{-1}$ as well as the total ice mass mixing ratio q_i in units of $1\,\mu\mathrm{g\,kg}^{-1}$

the computational cost of this additional procedure likely outweighs the benefit from an improved representation of ice particle properties.

While a high-resolution model is able to produce different particle properties within a single cloud, the global model often represents a cloud with only a few grid-boxes. Therefore the regions where the use of multiple free categories could improve the model results are these where the seeder-feeder mechanism or convective anvils contribute significantly to the ice water path. How important these situations are in the global context in ECHAM6-HAM2 will have to be investigated in future studies. Then the benefit from multiple free categories can be revisited.

Geosci. Model Dev. Discuss., https://doi.org/10.5194/gmd-2017-164
Manuscript under review for journal Geosci. Model Dev.
Discussion started: 14 August 2017

6 Conclusion

The single category scheme proposed by MM15 has been successfully implemented in the ECHAM6-HAM2 microphysics scheme. The structure of the original code has been reworked and the large-scale deposition, cloud cover, melting and rain production calculations have been adapted to comply with the prognostic ice category and a variable time-step. Numerical stability is achieved by sub-stepping the cloud microphysics and sedimentation routines with an attempt to keep computation time as low as possible by applying a nested sub-stepping approach. It has been shown that this yields reasonable accuracy for a simple sedimentation experiment.

The new scheme is evaluated against its forerunner within an idealized mixed-phase cloud simulation. We saw that different schemes to diagnose sedimentation of cloud ice strongly influence the microphysical process rates. The sub-stepping introduced in the new scheme allows cloud ice sedimentation to be calculated prognostically, thus eliminating this degree of freedom. At the same time, the continuous treatment of cloud ice with a single category no longer requires weakly constrained parameters like the threshold size for conversion of ice crystals to snow. Together, these factors make the new scheme more closely based on first principles which reduces its conceptual complexity and simplifies both model development and the interpretation of model results.

An important feature of the original P3 scheme are the rime variables that allow to predict the particle shape and density. An idealized seeder-feeder simulation showed that the influence of riming on particle properties can lead to substantial differences in microphysical process rates. However, the large gap between the resolved scales in ECHAM6-HAM2 and the scales on which hydrometeor collisions take place raises the question to which extent riming can be represented on a physical basis in this framework. The two additional prognostic variables might be unnecessary for the global model used in this study. To establish the rime fraction and density, up- and downdrafts need to be resolved on the scales of clouds. In the global model they are represented by the convection parameterization. It is therefore indispensable to include an elaborate microphysics scheme in the convection parameterization that is able to represent the co-existence of liquid water and ice which is not the case for the default scheme. While there have been approaches trying to improve this aspect in the past (Lohmann, 2008; Croft et al., 2012), assessing the rime fraction and density required for the P3 representation of cloud ice requires that the associated cloud parameters would also need to be prognosed within the convective parameterization of ECHAM6-HAM2.

We evaluated limitations of the single category scheme. The inability to distinguish particles from different sources, inherent to any bulk properties scheme, persists. At the core of this problem is the fact that it is not the ice particle properties themselves for which prognostic equations are solved but that they are diagnosed from the prognostic ice parameters. A solution has been proposed by Milbrandt and Morrison (2016) by using multiple free categories to give the particle properties themselves a prognostic flavor.

Reducing the number of weakly constrained parameters by going from a multi- to a single category scheme as well as fully resolving the ice formation pathway by the prognostic treatment of cloud ice are clear conceptual improvements over the original scheme. The level of sophistication to which the single category can be implemented in a global model remains to be seen. In the context of climate projections, the benefit from solving additional equations to represent riming, as is done in the

P3 scheme, or adding multiple free categories need to outweigh the associated computational cost. As a next step we will test the performance of the single category globally.

Code availability. The code of the cloud microphysics module (Fortran 95) is available upon request from the corresponding author or as part of the ECHAM6-HAMMOZ chemistry climate model through the HAMMOZ distribution web-page https://redmine.hammoz.ethz.ch/projects/hammoz.

Competing interests. The authors declare that they have no conflict of interest.

Acknowledgements. The ECHAM-HAMMOZ model is developed by a consortium composed of ETH Zurich, Max Planck Institut für Meteorologie, Forschungszentrum Jülich, University of Oxford, the Finnish Meteorological Institute and the Leibniz Institute for Tropospheric Research, and managed by the Center for Climate Systems Modeling (C2SM) at ETH Zurich. This project has been funded by the Swiss National Science Foundation (project number 200021_160177). We thank Hugh Morrison and Jason Milbrandt for sharing their ice particle property lookup tables that have been used for this study as well as their microphysics code as a reference and Jörg Wieder for his work related to the WBF process parameterization.

References

Abdul-Razzak, H. and Ghan, S. J.: A parameterization of aerosol activation: 2. Multiple aerosol types, J. geophys. res.-atmos., 105, 6837–6844, doi:10.1029/1999JD901161, 2000.

Abdul-Razzak, H., Ghan, S. J., and Rivera-Carpio, C.: A parameterization of aerosol activation: 1. Single aerosol type, J. geophys. res.-atmos., 103, 6123–6131, doi:10.1029/97JD03735, 1998.

Beheng, K.: A parameterization of warm cloud microphysical conversion processes, Atmos. res., 33, 193 – 206, doi:http://dx.doi.org/10.1016/0169-8095(94)90020-5, 11th International Conference on Clouds and Precipitation, Part II, 1994.

Bony, S., Stevens, B., Frierson, D. M. W., Jakob, C., Kageyama, M., Pincus, R., Shepherd, T. G., Sherwood, S. C., Siebesma, A. P., Sobel, A. H., Watanabe, M., and Webb, M. J.: Clouds, circulation and climate sensitivity, Nat. geosci., 8, 261–268, doi:10.1038/ngeo2398; 10.1038/ngeo2398, 2015.

Croft, B., Pierce, J. R., Martin, R. V., Hoose, C., and Lohmann, U.: Uncertainty associated with convective wet removal of entrained aerosols in a global climate model, Atmos. chem. phys., 12, 10 725–10 748, doi:10.5194/acp-12-10725-2012, 2012.

Eidhammer, T., Morrison, H., Mitchell, D., Gettelman, A., and Erfani, E.: Improvements in Global Climate Model Microphysics Using a Consistent Representation of Ice Particle Properties, J. climate, 30, 609–629, doi:10.1175/JCLI-D-16-0050.1, 2017.

Field, P. R. and Heymsfield, A. J.: Importance of snow to global precipitation, Geophys. res. lett., 42, 9512–9520, doi:10.1002/2015GL065497, 2015GL065497, 2015.

Gettelman, A. and Morrison, H.: Advanced Two-Moment Bulk Microphysics for Global Models. Part I: Off-Line Tests and Comparison with Other Schemes, J. climate, 28, 1268–1287, doi:10.1175/JCLI-D-14-00102.1, 2015.

Gettelman, A., Morrison, H., Santos, S., Bogenschutz, P., and Caldwell, P. M.: Advanced Two-Moment Bulk Microphysics for Global Models. Part II: Global Model Solutions and Aerosol-Cloud Interactions, J. climate, 28, 1288–1307, doi:10.1175/JCLI-D-14-00103.1, 2015.

Hope, C.: The $10 trillion value of better information about the transient climate response, Philos. t. roy. soc. A, 373, doi:10.1098/rsta.2014.0429, 2015.

Ickes, L., Welti, A., and Lohmann, U.: Classical nucleation theory of immersion freezing: sensitivity of contact angle schemes to thermodynamic and kinetic parameters, Atmos. chem. phys., 17, 1713–1739, doi:10.5194/acp-17-1713-2017, 2017.

Ickes, L., Welti, A., Hoose, C., and Lohmann, U.: Classical nucleation theory of homogeneous freezing of water: thermodynamic and kinetic parameters, Phys. chem. chem. phys., 17, 5514–5537, doi:10.1039/c4cp04184d, 2015.

Jensen, A. A. and Harrington, J. Y.: Modeling Ice Crystal Aspect Ratio Evolution during Riming: A Single-Particle Growth Model, J. atmos. sci., 72, 2569–2590, doi:10.1175/JAS-D-14-0297.1, 2015.

Kärcher, B. and Lohmann, U.: A parameterization of cirrus cloud formation: Homogeneous freezing of supercooled aerosols, J. geophys. res.-atm., 107, AAC 4–1–AAC 4–10, doi:10.1029/2001JD000470, 2002.

Kessler, E.: On the Distribution and Continuity of Water Substance in Atmospheric Circulations, Am. meteorol. soc. meteorol. monograph, 1969.

Khairoutdinov, M. and Kogan, Y.: A new cloud physics parameterization in a large-eddy simulation model of marine stratocumulus, Mon. weather rev., 128, 229–243, doi:10.1175/1520-0493(2000)128<0229:ANCPPI>2.0.CO;2, 2000.

Korolev, A. and Mazin, I.: Supersaturation of water vapor in clouds, J. atmos. sci., 60, 2957–2974, doi:10.1175/1520-0469(2003)060<2957:SOWVIC>2.0.CO;2, 2003.

Li, J.-L. F., Waliser, D. E., Chen, W.-T., Guan, B., Kubar, T., Stephens, G., Ma, H.-Y., Deng, M., Donner, L., Seman, C., and Horowitz, L.: An observationally based evaluation of cloud ice water in CMIP3 and CMIP5 GCMs and contemporary reanalyses using contemporary satellite data, J. geophys. res.-atmos., doi:10.1029/2012JD017640, 2012.

Lin, Y.-L., Farley, R. D., and Orville, H. D.: Bulk Parameterization of the Snow Field in a Cloud Model, J. clim. appl. meteorol., 22, 1065–1092, doi:10.1175/1520-0450(1983)022<1065:BPOTSF>2.0.CO;2, 1983.

Lohmann, U.: Possible Aerosol Effects on Ice Clouds via Contact Nucleation, J. atmos. sci., 59, 647–656, doi:10.1175/1520-0469(2001)059<0647:PAEOIC>2.0.CO;2, 2002.

Lohmann, U.: Global anthropogenic aerosol effects on convective clouds in ECHAM5-HAM, Atmos. chem. phys., 8, 2115–2131, doi:10.5194/acp-8-2115-2008, 2008.

Lohmann, U. and Diehl, K.: Sensitivity Studies of the Importance of Dust Ice Nuclei for the Indirect Aerosol Effect on Stratiform Mixed-Phase Clouds, J. atmos. sci., 63, 968–982, doi:10.1175/JAS3662.1, 2006.

Lohmann, U. and Roeckner, E.: Design and performance of a new cloud microphysics scheme developed for the ECHAM general circulation model, Climate Dynamics, 12, 557–572, doi:10.1007/BF00207939, http://dx.doi.org/10.1007/BF00207939, 1996.

Lohmann, U., Feichter, J., Chuang, C. C., and Penner, J. E.: Prediction of the number of cloud droplets in the ECHAM GCM, J. geophys. res.-atmos., 104, 9169–9198, doi:10.1029/1999JD900046, 1999.

Lohmann, U., Lüönd, F., and Mahrt, F.: An Introduction to Clouds: From the Microscale to Climate, Cambridge University Press, doi:10.1017/CBO9781139087513, 2016.

Lohmann, U., Spichtinger, P., Jess, S., Peter, T., and Smit, H.: Cirrus cloud formation and ice supersaturated regions in a global climate model, Environ. res. lett., 3, doi:10.1088/1748-9326/3/4/045022, 2008.

Marcolli, C.: Pre-activation of aerosol particles by ice preserved in pores, Atmos. chem. phys., 17, 1596–1623, doi:10.5194/acp-17-1595-2017, 2017.

Milbrandt, J. A. and Morrison, H.: Parameterization of Cloud Microphysics Based on the Prediction of Bulk Ice Particle Properties. Part III: Introduction of Multiple Free Categories, J. atmos. sci., 73, 975–995, doi:10.1175/JAS-D-15-0204.1, 2016.

Morrison, H. and Gettelman, A.: A New Two-Moment Bulk Stratiform Cloud Microphysics Scheme in the Community Atmosphere Model, Version 3 (CAM3). Part I: Description and Numerical Tests, J. climate, 21, 3642–3659, doi:10.1175/2008JCLI2105.1, 2008.

Morrison, H. and Milbrandt, J. A.: Parameterization of Cloud Microphysics Based on the Prediction of Bulk Ice Particle Properties. Part I: Scheme Description and Idealized Tests, J. atmos. sci., 72, 287–311, doi:10.1175/JAS-D-14-0065.1, 2015.

Muelmenstaedt, J., Sourdeval, O., Delanoe, J., and Quaas, J.: Frequency of occurrence of rain from liquid-, mixed-, and ice-phase clouds derived from A-Train satellite retrievals, Geophys. res. lett., 42, 6502–6509, doi:10.1002/2015GL064604, 2015.

Murakami, M.: Numerical Modeling of Dynamical and Microphysical Evolution of an Isolated Convective Cloud, J. meteorol. soc. jpn., Ser. II, 68, 107–128, doi:10.2151/jmsj1965.68.2_107, 1990.

Phillips, V. T. J., Demott, P. J., Andronache, C., Pratt, K. A., Prather, K. A., Subramanian, R., and Twohy, C.: Improvements to an Empirical Parameterization of Heterogeneous Ice Nucleation and Its Comparison with Observations, J. atmos. sci., 70, 378–409, doi:10.1175/JAS-D-12-080.1, 2013.

Rotstayn, L. D.: A physically based scheme for the treatment of stratiform clouds and precipitation in large-scale models. I: Description and evaluation of the microphysical processes, Q. j. roy. meteor. soc., 123, 1227–1282, doi:10.1002/qj.49712354106, 1997.

Sant, V., Lohmann, U., and Seifert, A.: Performance of a Triclass Parameterization for the Collision–Coalescence Process in Shallow Clouds, J. atmos. sci., 70, 1744–1767, doi:10.1175/JAS-D-12-0154.1, 2013.

Sant, V., Posselt, R., and Lohmann, U.: Prognostic precipitation with three liquid water classes in the ECHAM5–HAM GCM, Atmos. chem. phys., 15, 8717–8738, doi:10.5194/acp-15-8717-2015, 2015.

Schneider, T., Teixeira, J., Bretherton Christopher, S., Brient, F., Pressel Kyle, G., Schär, C., and Siebesma A., P.: Climate goals and computing the future of clouds, Nat. clim. change, 7, 3–5, doi:10.1038/nclimate3190, 2017.

Seifert, A. and Beheng, K. D.: A two-moment cloud microphysics parameterization for mixed-phase clouds. Part 1: Model description, Meteorol. atmos. phys., 92, 45–66, doi:10.1007/s00703-005-0112-4, 2006.

Stevens, B., Giorgetta, M., Esch, M., Mauritsen, T., Crueger, T., Rast, S., Salzmann, M., Schmidt, H., Bader, J., Block, K., Brokopf, R., Fast, I., Kinne, S., Kornblueh, L., Lohmann, U., Pincus, R., Reichler, T., and Roeckner, E.: Atmospheric component of the MPI-M Earth System Model: ECHAM6, J. adv. model. earth sy., 5, 146–172, doi:10.1002/jame.20015, 2013.

Stevens, B., Sherwood, S. C., Bony, S., and Webb, M. J.: Prospects for narrowing bounds on Earth's equilibrium climate sensitivity, Earths future, 4, 512–522, doi:10.1002/2016EF000376, 2016EF000376, 2016.

Stocker, T., Qin, D., Plattner, G.-K., Alexander, L., Allen, S., Bindoff, N., Breon, F.-M., Church, J., Cubasch, U., Emori, S., Forster, P., Friedlingstein, P., Gillett, N., Gregory, J., Hartmann, D., Jansen, E., Kirtman, B., Knutti, R., Krishna Kumar, K., Lemke, P., Marotzke, J., Masson-Delmotte, V., Meehl, G., Mokhov, I., Piao, S., Ramaswamy, V., Randall, D., Rhein, M., Rojas, M., Sabine, C., Shindell, D., Talley, L., Vaughan, D., and Xie, S.-P.: Technical Summary, book section TS, p. 33–115, doi:10.1017/CBO9781107415324.005, 2013.

Sundqvist, H.: Parameterization scheme for non-convective condensation including prediction of cloud water-content, Q. j. roy. meteor. soc., 104, 677–690, doi:10.1256/smsqj.44109, 1978.

Sundqvist, H., Berge, E., and Kristjansson, J.: Condensation and cloud parameterization studies with a mesoscale numerical weather prediction model, Mon. weather rev., 117, 1641–1657, doi:10.1175/1520-0493(1989)117<1641:CACPSW>2.0.CO;2, 1989.

Tan, I. and Storelvmo, T.: Sensitivity Study on the Influence of Cloud Microphysical Parameters on Mixed-Phase Cloud Thermodynamic Phase Partitioning in CAM5, J. atmos. sci., 73, 709–728, doi:10.1175/JAS-D-15-0152.1, 2016.

Tan, I., Storelvmo, T., and Zelinka, M. D.: Observational constraints on mixed-phase clouds imply higher climate sensitivity, Science, 352, 224–227, doi:10.1126/science.aad5300, 2016.

Tiedtke, M.: A Comprehensive Mass Flux Scheme for Cumulus Parameterization in Large-Scale Models, Mon. weather rev., 117, 1779–1800, doi:10.1175/1520-0493(1989)117<1779:ACMFSF>2.0.CO;2, 1989.

Tompkins, A. M.: A Prognostic Parameterization for the Subgrid-Scale Variability of Water Vapor and Clouds in Large-Scale Models and Its Use to Diagnose Cloud Cover, J. atmos. sci., 59, 1917–1942, doi:10.1175/1520-0469(2002)059<1917:APPFTS>2.0.CO;2, 2002.

Welti, A., Kanji, Z. A., Lueoend, F., Stetzer, O., and Lohmann, U.: Exploring the Mechanisms of Ice Nucleation on Kaolinite: From Deposition Nucleation to Condensation Freezing, J. atmos. sci., 71, 16–36, doi:10.1175/JAS-D-12-0252.1, 2014.

Zhang, K., O'Donnell, D., Kazil, J., Stier, P., Kinne, S., Lohmann, U., Ferrachat, S., Croft, B., Quaas, J., Wan, H., Rast, S., and Feichter, J.: The global aerosol-climate model ECHAM-HAM, version 2: sensitivity to improvements in process representations, Atmos. chem. phys., 12, 8911–8949, doi:10.5194/acp-12-8911-2012, 2012.